

Journal Pre-proof

A carbohydrate-binding protein from the edible *Lablab* beans effectively blocks the infections of influenza viruses and SARS-CoV-2

Yo-Min Liu, Md. Shahed-Al-Mahmud, Xiaorui Chen, Ting-Hua Chen, Kuo-Shiang Liao, Jennifer M. Lo, Yi-Min Wu, Meng-Chiao Ho, Chung-Yi Wu, Chi-Huey Wong, Jia-Tsong Jan, Che Ma

PII: S2211-1247(20)31001-9

DOI: <https://doi.org/10.1016/j.celrep.2020.108016>

Reference: CELREP 108016

To appear in: *Cell Reports*

Received Date: 3 March 2020

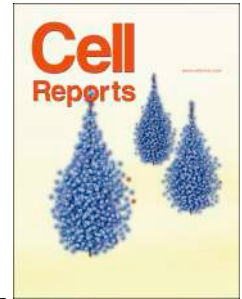
Revised Date: 9 June 2020

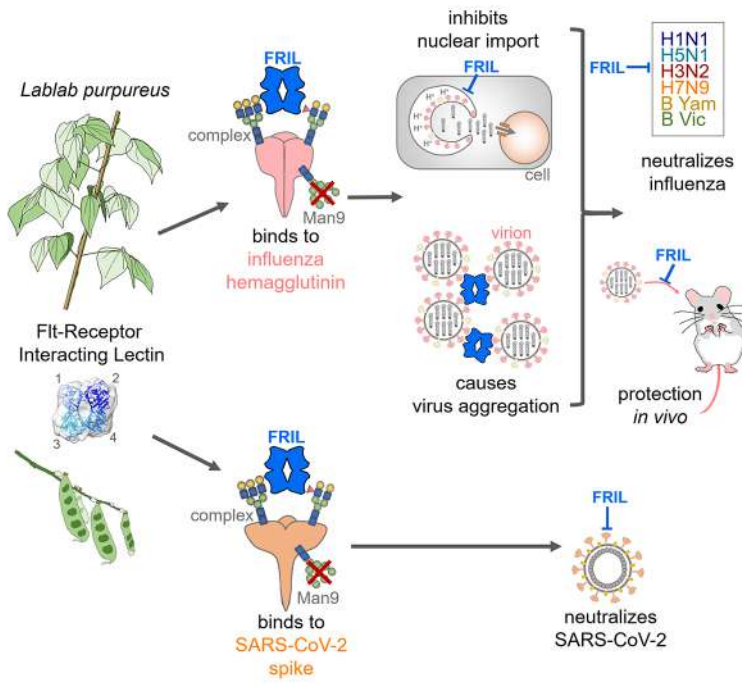
Accepted Date: 17 July 2020

Please cite this article as: Liu, Y.-M., Shahed-Al-Mahmud, M., Chen, X., Chen, T.-H., Liao, K.-S., Lo, J.M., Wu, Y.-M., Ho, M.-C., Wu, C.-Y., Wong, C.-H., Jan, J.-T., Ma, C., A carbohydrate-binding protein from the edible *Lablab* beans effectively blocks the infections of influenza viruses and SARS-CoV-2, *Cell Reports* (2020), doi: <https://doi.org/10.1016/j.celrep.2020.108016>.

This is a PDF file of an article that has undergone enhancements after acceptance, such as the addition of a cover page and metadata, and formatting for readability, but it is not yet the definitive version of record. This version will undergo additional copyediting, typesetting and review before it is published in its final form, but we are providing this version to give early visibility of the article. Please note that, during the production process, errors may be discovered which could affect the content, and all legal disclaimers that apply to the journal pertain.

© 2020





Journal Pre-proof

1
2
3
4
5
6
7
8
9
10
11
12
13
14
15
16
17
18
19
20
21
22
23
24
25
26
27
28
29
30

A carbohydrate-binding protein from the edible *Lablab* beans effectively blocks the infections of influenza viruses and SARS-CoV-2

Yo-Min Liu^{1,2}, Md. Shahed-Al-Mahmud¹, Xiaorui Chen¹, Ting-Hua Chen¹,
Kuo-Shiang Liao¹, Jennifer M. Lo¹, Yi-Min Wu³, Meng-Chiao Ho³, Chung-Yi
Wu¹, Chi-Huey Wong¹, Jia-Tsong Jan¹, Che Ma^{1,*}

¹ Genomics Research Center, Academia Sinica, Taipei 115, Taiwan.

² Institute of Microbiology and Immunology, National Yang Ming University, Taipei 112, Taiwan.

³ Institute of Biological Chemistry and Cryo-EM center, Academia Sinica, Taipei 115, Taiwan

* Lead contact. Correspondence and requests for materials should be addressed to C.M. (email: cma@gate.sinica.edu.tw)

31 **Summary**

32 The influenza virus hemagglutinin (HA) and coronavirus spike (S) protein mediate
33 virus entry. HA and S proteins are heavily glycosylated, making them potential targets
34 for carbohydrate binding agents such as lectins. Here we show that the lectin FRIL,
35 isolated from hyacinth beans (*Lablab purpureus*), has anti-influenza and
36 anti-SARS-CoV-2 activity. FRIL can neutralize 11 representative human and avian
37 influenza strains at low nanomolar concentrations, and intranasal administration of
38 FRIL is protective against lethal H1N1 infection in mice. FRIL binds preferentially to
39 complex type N-glycans, and neutralizes viruses that possess complex type N-glycans
40 on their envelopes. As a homotetramer, FRIL is capable of aggregating influenza
41 particles through multivalent binding and trapping influenza virions in cytoplasmic
42 late endosomes, preventing their nuclear entry. Remarkably, FRIL also effectively
43 neutralizes SARS-CoV-2, preventing viral protein production and cytopathic effect in
44 host cells. These findings suggest potential application of FRIL for prevention and/or
45 treatment of influenza and COVID-19.

46

47 Keywords: lectin, influenza, coronavirus, SARS-CoV-2, antiviral, N-glycosylation

48

49 Introduction

50 Each year, influenza virus infections cause more than half a million deaths worldwide
51 (Lozano et al., 2012). Several neuraminidase (NA) inhibitors and a polymerase acidic
52 protein (PA) inhibitor are available as therapeutics, with a third class, M2 inhibitors,
53 obsolete due to widespread resistance (Heo, 2018). A number of monoclonal
54 antibodies that target the viral entry glycoprotein hemagglutinin (HA) are also in
55 various stages of clinical development (Koszalka et al., 2017). However, due to the
56 virus' high mutational capacity, the spread of NA and PA inhibitor-resistant mutants
57 are a concern (Yang et al., 2011, Imai et al., 2020), and mutations have been shown to
58 decrease antibody binding to HA resulting in reduced efficacy (Wu et al., 2014).
59 Antiviral strategies which aim at components of the virus particle such as
60 post-translational glycosylations that incur a higher fitness cost for mutation can be
61 advantageous for combating influenza.

62

63 A variety of complex, high mannose and hybrid type N-glycans are attached by
64 cellular mechanisms to influenza surface glycoproteins. They are essential for correct
65 protein folding and trafficking, affect HA receptor binding, and help the influenza
66 virus evade host antibody detection through the shielding of immunogenic epitopes
67 (Wu et al., 2017). The latter phenomenon of "glycan shield" has been proposed as to
68 why most circulating human influenza viruses, in response to rising immunity in the
69 population, have steadily increased the number of glycosylation sites on their HAs
70 (Tate et al., 2014). The essential role of N-glycans on viral fitness, coupled with
71 influenza virus' limited ability to alter their composition, makes viral surface glycans
72 a potential target for antiviral strategy.

73

74 Glycans are also commonly found for other enveloped viruses, of which the
75 glycosylation profile varies among the surface proteins of each virus. The novel
76 coronavirus severe acute respiratory syndrome coronavirus 2 (SARS-CoV-2),
77 responsible for the currently ongoing COVID-19 pandemic that has caused over 10
78 million reported cases worldwide and over five hundred thousand deaths, also
79 contains the heavily-glycosylated surface glycoprotein spike (S) protein. This
80 glycoprotein gives the virion its namesake crown-like appearance and also mediates
81 virus attachment and entry into the host cell. The SARS-CoV-2 spike gene encodes 22
82 N-linked glycosylation sites per monomer, the majority of which feature complex or
83 hybrid type glycans (Watanabe et al., 2020). Since no vaccines or therapeutics are
84 currently available for COVID-19, studies of SARS-CoV-2 as a prime target for
85 anti-viral lectins, especially those that bind to complex type N-glycans, are of special
86 interest and substantial importance.

87

88 A number of lectins with antiviral properties have been discovered, with the vast
89 majority being high-mannose binding lectins directed against the heavily-glycosylated
90 human immunodeficiency virus (HIV) (Mitchell et al., 2017). Griffithsin (GRFT), a
91 lectin isolated from the red algae *Griffithsia* sp., is currently in clinical trials as a
92 topical vaginal gel for the prevention of HIV (Giancetti et al., 2019). A major
93 obstacle for exogenous lectin treatment *in vivo* is their potential toxicity, as they may
94 also recognize sugar moieties on host cells. So far, only the high-mannose binding
95 lectins Cyanovirin (CVN) and H84T Banlec have been shown to be protective against
96 influenza virus challenge in mice by intranasal administration (Smee et al., 2008,
97 Swanson et al., 2015). H84T Banlec is also protective intraperitoneally
98 (Covés-Datson et al., 2020). Lectins that inhibit influenza virus and bind to complex
99 type glycans include the *Nicotiana tabacum* agglutinin and *Urtica dioica* agglutinin
100 (Gordts et al., 2015, Balzarini et al., 1992).

101

102 For coronaviruses, several mannose, GlcNAc, and mannose/glucose specific
103 exogenous lectins can inhibit severe acute respiratory syndrome coronavirus
104 (SARS-CoV), Middle East respiratory syndrome coronavirus (MERS-CoV) and other
105 mammalian and avian coronaviruses (O'Keefe et al., 2010, Millet et al., 2016, Kumaki
106 et al., 2011, Hsieh et al., 2010, Greig and Bouillant, 1977), by interfering with
107 coronavirus entry and egress through interactions with the viral spike protein
108 (Keyaerts et al., 2007). However, no report on the effectiveness of anti-viral lectins
109 against SARS-CoV-2 have been made.

110

111 *Lablab purpureus*, previously known as *Dolichos lablab* and commonly referred to as
112 the hyacinth bean or lablab bean, is a legume in the Fabaceae family, mentioned in the
113 Chinese traditional medicine text *Compendium of Materia Medica* as having
114 properties of 'strengthening the spleen and reducing dampness'. *Dolichos lablab*
115 lectin 1 (DLL-I) is a glucose/mannose lectin (Mo et al., 1999) isolated from the
116 hyacinth bean that has also been referred to as Flt3 Receptor Interacting Lectin
117 (FRIL), after Colucci *et al* discovered it having the unique property of sustaining
118 hematopoietic progenitor cells in suspension culture by binding to cellular Flt3
119 receptors (Colucci et al., 1999). FRIL has also been shown to preserve neural
120 progenitor cells, and evokes anti-tumor activity by reducing tumor neoangiogenesis
121 through immunomodulation (Yao et al., 2008, Vigneshwaran et al., 2017). It is a
122 typical legume lectin that has a 48% sequence identity to the well-known
123 concanavalin A (ConA), with a similar β -prism type-II fold and one carbohydrate
124 binding domain per monomer. Previous studies have suggested that FRIL is a

125 glucose/mannose specific lectin based on its affinity for monosaccharides mannose,
126 glucose, and N-acetylglucosamine, with a strong preference for the α -anomeric
127 configuration (Mo et al., 1999). However, no study has been done on FRIL's binding
128 to higher-order sugars such as the N-glycans commonly found on cell or viral
129 glycoproteins; nor has FRIL been reported to have anti-viral activity.

130

131 Our current research stemmed from a screening of various ingredients used in Chinese
132 traditional medicine for microneutralization activity against the influenza virus. From
133 this screening, we discovered that the aqueous extract from *Lablab purpureus* has
134 potent anti-influenza activity against a broad spectrum of influenza strains, and this
135 activity was abrogated by heat or proteinase K treatment. The unexpected emergence
136 of COVID-19 in the midst of our ongoing study compelled us to also explore its
137 effects on SARS-CoV-2. Here we elucidate the protein FRIL isolated from this extract
138 is responsible for our observed neutralization effect, and characterize its neutralization
139 breadth, potency, ligand binding and stoichiometry, as well as its mechanism of
140 action.

141

142 **Results**

143 ***Lablab* extract neutralizes influenza virus.**

144 First, we assessed the microneutralization (MN) ability of serially-diluted crude
145 aqueous extract of *Lablab purpureus* seeds (Fig. 1A) against four influenza vaccine
146 strains spanning both group 1 and group 2 influenza A viruses, including
147 A/California/7/2009-like (H1N1 X181), A/Vietnam/1194/2004-like (H5N1 RG14),
148 A/Victoria/361/2011-like (H3N2 IVR-165), and A/Shanghai/2/2013-like (H7N9
149 RG32A). Results showed that *Lablab* crude extract exhibited neutralization ability
150 against all four strains tested (Fig. 1B).

151

152 **FRIL is isolated and characterized from *lablab* extract.**

153 In order to isolate the agent in the aqueous extract of *Lablab purpureus* seeds
154 responsible for the observed influenza MN effect, we did sequential protein
155 fractionations including ammonium sulfate precipitation, anion-exchange
156 chromatography, size-exclusion and affinity chromatography with Cibacron Blue
157 beads. In each step, fractions with the highest MN titer against H5N1 RG14 were
158 selected to proceed to the next step. Finally, five SDS-PAGE bands ranging from 10
159 to 20 kDa remain, resisting any further attempts at separation. The final fraction
160 containing these five bands appeared as a single protein band when run on a native
161 PAGE (Fig. 1C). Additionally, this band was excised and eluted from the native PAGE,
162 and the eluted protein retained neutralization activity against RG14. Mass
163 spectrometry analysis revealed these five bands contained peptide sequences identical
164 to the *Lablab purpureus* Flt-receptor interacting lectin (FRIL) (Colucci et al., 1999)
165 and *Dolichos lablab* lectin (DLL, later named DLL-I) peptide (Gowda et al., 1994),
166 with the four higher kDa bands corresponding to FRIL differentially-digested and
167 N-glycosylated α subunit and the lowest band corresponding to the β subunit (B et al.,
168 2014).

169

170 FRIL has one carbohydrate-binding domain (CBD) per monomer, but there have been
171 conflicting reports on whether FRIL is a dimer or tetramer in solution (Mo et al., 1999,
172 Gowda et al., 1994, Guran et al., 1983). To determine the oligomeric state of FRIL,
173 we employed size-exclusion chromatography with multiple angle light scattering
174 (SEC-MALS), dynamic light scattering (DLS), and negative stain electron
175 microscopy (EM). SEC-MALS analysis suggest that our purified FRIL forms a 112.1
176 kDa tetramer in solution (Fig. 1D). Using negative staining electron microscopy, a
177 tetrameric electron density map of ~ 27 Å resolution was seen (Fig. 1E, supplementary
178 Fig. S1A), similar to its previously reported crystal structure (Hamelryck et al., 2000).
179 DLS results also showed that FRIL's size resembles known tetrameric legume lectin

180 ConA, which has a similar tertiary structure as FRIL (supplementary Fig. S1B).

181

182 **FRIL has potent anti-influenza activity *in vitro* and *in vivo*.**

183 The anti-influenza activity of FRIL *in vitro* was assessed with plaque reduction assay
184 and MN. FRIL exhibited a 50% plaque reduction neutralization test (PRNT₅₀) value
185 of 0.697 µg/ml against X181, similar to its MN half maximal effective concentration
186 (EC₅₀) of 0.74 µg/ml (Fig. 2A, 2B, supplementary Fig S2A). Next, we explored the
187 MN breadth of the purified FRIL with a representative panel of 11 influenza viruses
188 spanning group 1 (H1N1), group 2 (H3N2) and influenza B (Yamagata and Victoria
189 linages), along with avian strains of H7N9 and H5N1. The EC₅₀ results were
190 compared with the broadly-neutralizing influenza antibody (bnAb) FI6v3 (Corti et al.,
191 2011). With the exception of the laboratory strain A/Puerto Rico/8/1934 (PR8), FRIL
192 was able to achieve low nanomolar levels of EC₅₀ against group 1 viruses (H1N1 and
193 H5N1) and H3N2. FRIL also had nanomolar neutralization titers against H7N9 and
194 influenza B, ranging from an EC₅₀ of 8.39 nM for a B/Malaysia/2506/2004-like virus
195 to 231.4 nM for a B/Florida/4/2006-like virus (Fig 2C, supplementary Fig S2B). The
196 EC₅₀ values of FI6v3 were in a similar range to what has been previously reported
197 (Corti et al., 2011). In addition, a FRIL MN experiment comparing either
198 egg-produced or MDCK cell-produced X181 viruses shows that the source of virus
199 does not affect FRIL's EC₅₀ (supplementary Fig S2C).

200

201 Having demonstrated FRIL's anti-influenza effects *in vitro*, we next evaluated FRIL's
202 *in vivo* activity by intranasal administration in mice. FRIL was first given intranasally
203 to 10 BALB/c mice 4 hrs before intranasal infection with 5 LD₅₀ (median lethal dose)
204 of X181 virus. Afterwards, FRIL was administered every 12 hours for 8 days, and
205 survival and body weight were monitored for 21 days post-infection (Fig. 2D). We
206 found that 58.6 µg/day (2.93 mg/kg/day) FRIL intranasal treatment offered protection
207 in 7 out of 10 mice, with the three deaths delayed compared to PBS controls. At 5.86
208 µg/day (0.29 mg/kg/day) treatment, the median time of death was also significantly
209 delayed by 4 days (Fig. 2E, 2F), though only 1/10 mice survived.

210

211 Taken together, these results demonstrate that the purified FRIL possess
212 broad-spectrum anti-influenza activity *in vitro* and has dose-dependent anti-viral
213 activity when given intranasally *in vivo*.

214

215 **FRIL only neutralize influenza viruses with complex type N-glycans.**

216 Although previous reports have shown FRIL to be a mannose/glucose-specific lectin,
217 its affinity to higher-order sugar structures found on influenza envelope proteins has

218 not been studied. To explore what types of oligosaccharides FRIL binds to, we created
219 differentially-glycosylated egg-based influenza viruses of H1N1 X181 by subjecting
220 them to treatment by the mannosidase I inhibitor kifunensine (KIF) during seeding
221 into allantoic cavity of eggs, followed by a high mannose-cleaving endoglycosidase H
222 (endo H) after harvest (Tseng et al., 2019). Four types of virus particles were thus
223 created: no treatment (both complex and high mannose-type glycans exist on the virus
224 surface naturally), KIF-treated (high mannose only), endo H-treated (complex glycans
225 remain intact, high mannose glycans digested down to single GlcNAc) and KIF/endo
226 H-treated (single GlcNAc only) (Fig. 3A). These viruses were then purified by
227 sucrose density gradient centrifugation, and its N-glycan constituency confirmed by
228 glycopeptide analysis with tandem mass spectrometry (supplementary Fig S3A).

229

230 We tested the binding of FRIL to these three types of differentially-glycosylated
231 viruses by FRIL immunoblotting (where lysed whole viruses were blotted onto a
232 PVDF membrane, then probed with FRIL) and live virus ELISA. Immunoblotting
233 showed FRIL binds primarily to hemagglutinin (HA), the glycoprotein that mediates
234 virus attachment and entry (Fig. 3B). Surprisingly, FRIL bound to non-treated, mostly
235 complex type virus particles at a higher intensity than KIF-treated high mannose
236 viruses, which is different from the oligosaccharide binding affinity of most other
237 known antiviral lectins (Fig. 3B). In a live virus ELISA, (supplementary Fig S3B)
238 FRIL also showed significantly higher binding to complex type particles, in spite of
239 possible interference by glycolipids and other non-specific components of the
240 glycocalyx in this assay. This preference for complex type glycans is also reflected in
241 MN assays: FRIL only shows neutralization against non-treated and endo H-treated
242 viruses containing complex type sugars, but not against high mannose and single
243 GlcNAc viruses (Fig. 3C). In contrast, the well-documented high mannose binding
244 lectin ConA had the highest neutralization titers against KIF-treated viruses (Fig. 3D),
245 and bnAb FI6v3 (an HA stem-specific antibody possibly affected by steric hindrance
246 of N-glycans near its epitope (Magadan et al., 2014)) showed the best neutralization
247 activity against virus particles that contained only a single GlcNAc (Fig. 3E).

248

249 To further investigate this interesting phenomenon, we utilized glycan array analysis
250 using fluorescent dye Cy3-labeled FRIL (Fig. 3F). FRIL demonstrated the best
251 binding to complex type N-glycans with α 1-3 or α 1-4 fucosylated sub-terminal
252 GlcNAc, including Gal β 1-4(Fuc α 1-3)GlcNAc β 1-2Man-R (Lewis
253 X/SSEA-1/CD15-carrying N-glycans) and Gal β 1-4(Fuc α 1-4)GlcNAc β 1-2Man-R,
254 ranging from 21,085,870 to 6,257,633 relative fluorescent units (RFU). Slightly
255 weaker binding was seen on non-terminally-fucosylated complex and hybrid type

256 N-glycans (1,437,565 to 463,152 RFU), as well as its previously-documented binding
257 to the singular mannose residue (827,081 RFU) and GlcNAc-linked trimannose
258 (142,360 RFU). Signal from oligomannose residues Man9 (49,933 RFU) and Man5
259 (64,093 RFU), or Lewis X (39,490 RFU) and Lewis A (42,606 RFU) antigens that
260 were not attached to the N-glycan trimannose core were no higher than other
261 unrelated glycan structures. Terminal desialylation, as would be anticipated from
262 influenza neuraminidase (NA) activity, did not appear to affect FRIL binding
263 (supplementary Fig S3C). In contrast, Cy3-labeled ConA exhibited the strongest
264 binding to oligomannose structures such as Man3, Man5 and Man9. The result of
265 direct Cy3 labeling was confirmed by using polyclonal anti-FRIL antibodies
266 (supplementary Fig S3D).

267

268 In summary, our glycan array analysis supports our assays with
269 differentially-glycosylated influenza viruses, indicating that FRIL binds preferentially
270 to complex type N-glycans, and only neutralize viruses with complex type glycans on
271 their surface. Compared to other high-mannose-binding anti-viral lectins in previous
272 studies, such as Griffithsin (GRFT), Cyanovirin (CVN) and H84T Banlec, the
273 complex-type-binding FRIL may have an advantage in targeting viral glycoproteins
274 whose complex type glycans are in majority, such as HA of H1N1, Spike of
275 SARS-CoV-2, etc. The molecular mechanism underlying such a binding preference is,
276 however, yet to be revealed.

277

278 **FRIL sequesters influenza virions in late endosome and prevents nuclear entry.**

279 Due to the surprising finding that FRIL's oligosaccharide preference is different from
280 most known antiviral lectins, we were interested in its antiviral mechanism. First, a
281 competitive microneutralization inhibition assay using monosaccharides shows that
282 the two sugars which can inhibit FRIL hemagglutination, α -methylmannopyranoside
283 and D-glucose, were also able to inhibit FRIL MN (Fig. 4A), suggesting that FRIL's
284 observed neutralization effect is dependent on its carbohydrate binding function.
285 Second, pre-treatment of cells with either FRIL or virus, followed by 18 hours of
286 incubation with the opposite agent (without either coming into direct contact with one
287 another) both failed to neutralize the influenza virus (Fig. 4B), confirming that FRIL
288 is an inhibitor of virus entry, and must bind directly to the virus particle.

289

290 Influenza virus cell entry includes the sequential steps of virus attachment,
291 endocytosis, uncoating, and nuclear import. To test whether FRIL blocks attachment,
292 we employed a FRIL hemagglutination inhibition assay (HAI) against H1N1, H3N2,
293 H5N1 and H7N9 viruses (supplementary Fig. S4A). In all four strains, no HAI was

294 observed up to 11.7 $\mu\text{g/ml}$ FRIL. An ELISA done on influenza NP in MDCK cells
295 given 1 hour to bind with virus also showed no significant difference in virus
296 attachment whether FRIL was added or not (supplementary Fig. S4B). We therefore
297 conclude FRIL does not inhibit influenza virus attachment. The next step after virus
298 attachment is cell endocytosis, a process that can be delayed by lowering the
299 temperature to 4 °C (Matlin et al., 1981). To confirm that FRIL's neutralization effect
300 occurs after virus attachment, virus particles were added to the cell surface at low
301 temperatures so that attachment takes place but endocytosis is inhibited, and FRIL
302 was then added to the virus-attached cells (Fig. 4C). Under this condition FRIL
303 exhibited a similar neutralization EC_{50} compared with when the lectin and virus were
304 mixed and added to cells together (EC_{50} 4.25 $\mu\text{g/ml}$ and 2.35 $\mu\text{g/ml}$, respectively). In
305 contrast, giving the virus 1 hour at 37°C to be endocytosed before FRIL treatment
306 results in a complete loss of neutralization, indicating that FRIL exerts its antiviral
307 effect after virus attachment, only after being in contact with the virus before its
308 endocytosis and subsequent infection (Fig. 4C).

309

310 Finally, we followed the progression of the influenza virus after its endocytosis into
311 the host cell by tracking viral NP protein with immunofluorescence staining by
312 anti-NP antibody (Fig. 4D, E). Multiple-round infections after initial addition of virus
313 to the slide were inhibited by a lack of TPCK-trypsin in cell culture medium. In
314 non-treated controls (PBS), the virus is carried by endosomes to the perinuclear
315 region at 1 hour post-infection (hpi), where the virus would then undergo endosomal
316 acidification and HA-mediated viral fusion. At 4 hpi the viral ribonucleoprotein
317 complex (vRNP, including NP) for the non-treated control was observed in the
318 nucleus, where influenza transcription and replication takes place. Production of new
319 NP in the cytoplasm was seen at 8 and 12 hpi, and widespread cell death occurred at
320 24 hpi for the control group. In contrast, 33 $\mu\text{g/ml}$ FRIL treatment caused retention of
321 NP signal in the perinuclear region for up to 12 hpi. Staining with the late
322 endosomal/lysosomal marker LAMP-1 confirmed that NP signal remained in late
323 endosomes/lysosomes (Fig. 4F). NP signals became weaker by 24 hpi (Fig.4D),
324 presumably due to eventual breakdown in lysosomes. 33 $\mu\text{g/ml}$ of ConA treatment
325 also exhibited a pattern of numerous NP vacuoles sequestered in the perinuclear
326 region at 4 hpi (supplementary Fig. S4C), while treatment of MDCK cells with FRIL
327 alone in the absence of influenza infection found that the FRIL protein binds mostly
328 to the cell membrane (supplementary Fig. S4D). FRIL immunoblotting under different
329 pH conditions was used to confirm that FRIL is active at endosomal pH
330 (supplementary Fig. S4E). A trypsin susceptibility assay done with recombinant HA
331 showed that unlike the HA stem-targeting antibody FI6, FRIL does not prevent

332 pH-dependent HA conformational change (supplementary Fig. S4F).

333

334 Overall, our results establish that FRIL exerts its anti-influenza effect by binding to
335 the virus, halting its infection in the late endosome/lysosome and preventing its
336 nuclear import through ways other than affecting HA conformational change for virus
337 fusion.

338

339 **FRIL displays multiple layers or dimensions of multivalency.**

340 During our immunofluorescence staining of influenza NP, we noticed granules of
341 large, intense anti-NP signal in our FRIL-treated group but not in the PBS-treated
342 control. As FRIL is a tetramer (Fig. 1D, E) capable of multivalent cross-linking
343 (Hamelryck et al., 2000) and erythrocyte aggregation (supplementary Fig. S4A), we
344 suspect these granules are influenza virion/FRIL aggregates displaying multiple
345 dimensions of multivalency characteristic of potent anti-viral lectins (Lusvarghi et al.,
346 2016).. To explore this possibility, we first performed DLS analysis on purified
347 influenza X181 virus particles that were then treated with 1.5 µg/ml to 490 µg/ml of
348 FRIL. Starting at 22 µg/ml, an increase in particle diameter intensity distribution can
349 be observed (147.6 nm ± 38.4 at 0 µg/ml increased to 202.7 nm ± 80.2 at 22 µg/ml
350 of FRIL), indicating the formation of aggregates (Fig. 5C). In contrast, no such
351 aggregation was observed for KIF- and endo H-treated viruses (with only a single
352 GlcNAc at each N-glycosylation site) even at the highest concentration used (145.2
353 nm ± 39.7 at 0 µg/ml compared with 151.2 nm ± 47.0 at 490 µg/ml of FRIL)
354 (supplementary Fig S5).

355

356 Under negative stain electron microscopy, large three-dimensional aggregations of
357 overlapping influenza X181 particles were observed at 150 µg/ml FRIL concentration,
358 while little aggregation was seen in untreated virus particles (Fig. 5B). Quantification
359 of aggregation was done by manually counting virus particles in close proximity to
360 one another (Fig. 5C). We observed a dose-dependent increase in the percentage of
361 aggregates up to 32 µg/ml FRIL, though concentrations higher than that formed
362 densely-packed clumps of layered viruses that make it difficult to quantify individual
363 particles visually.

364

365 These results indicate that FRIL's outward projection of four CBDs are capable of
366 bridging multiple virus particles and creating large, 3-dimensional aggregations of
367 influenza virion at 32~150 µg/ml. The clustering of virions may partially explain the
368 FRIL-mediated inhibitory mechanism of viral entry and nuclear import, and will serve
369 as the first step towards a molecular understanding for these events. Furthermore,

370 endogenous airway lectins SP-D and MBL are known to aggregate influenza virus
371 particles to facilitate viral clearance by the immune system *in vivo* (Hartshorn et al.,
372 1997), it is possible FRIL has a similar effect.

373

374 **FRIL exhibits potent neutralization of SARS-CoV-2, but not HIV.**

375 We assessed the antiviral activity of FRIL against the SARS-CoV-2 strain
376 hCoV-19/Taiwan/NTU04/2020 with microscopic observation of cytopathic effect
377 (CPE), a plaque reduction neutralization assay visualized by crystal violet staining,
378 and MN assay with polyclonal anti-SARS-CoV-2 nucleoprotein (N). From direct
379 observation of CPE, the Vero cell monolayer was morphologically unaffected by
380 virus introduction down to 6.25 µg/ml of FRIL, with focal CPE appearing as the FRIL
381 concentration dropped to 3.13~1.56 µg/ml, and widespread cell detachment below
382 0.39 µg/ml (Fig. 6A). In plaque reduction neutralization assay, FRIL exhibited a
383 PRNT₅₀ value of 0.71 µg/ml (6.36 nM) against hCoV-19/Taiwan/NTU04/2020 (Fig.
384 6B, supplementary Fig. S6B) after 4 days of incubation, similar to its MN EC₅₀ of
385 0.80 µg/ml (7.15 nM) (Fig. 6C).

386

387 Furthermore, we explored the effect of FRIL on viral protein production over time
388 inside Vero E6 cells by using polyclonal anti-SARS-CoV-2 N protein and
389 SARS-CoV-2 S protein antibodies at 1, 2, 4, 8, 16 and 24 hours post-infection (Fig.
390 6D, E, supplementary Fig. S6C). In non-FRIL-treated controls (PBS), viral N protein
391 signals were observed inside cell punctae starting at 4 hpi, and the percentage of cells
392 that stained strongly with N protein signal in its cytosol (signifying new N protein
393 production) steadily increased from 8 hpi onwards. In contrast, very little N protein
394 production was seen inside FRIL-treated cells up to 24 hpi. Viral S protein displayed
395 a similar trend, though the patchy distribution of membrane-bound S protein makes
396 them harder to quantify.

397

398 In contrast to FRIL's potent effects against SARS-CoV-2, MN using pseudotyped
399 HIV-1 JR-FL virus only yielded a moderate EC₅₀ of 8.41 µg/ml (74.96 nM,
400 supplementary Fig. S6A), and more importantly, FRIL was not able to achieve >90%
401 neutralization even at the highest concentration used (316 µg/ml).

402

403 **FRIL binds to SARS-CoV-2 spike protein**

404 ELISA was used to determine FRIL's binding affinity to recombinant SARS-CoV-2
405 spike protein produced in HEK293T (with native glycosylation) and HEK293S
406 (GnTI-, high mannose N-glycosylation only) cells. We found FRIL was able to bind to
407 recombinant S protein at concentrations as low as 10 ng/ml (89.1 picomole), and the

408 binding to S proteins with predominantly complex type N-glycans (native
409 glycosylation) is 30 times stronger than those with only high mannose glycans (Fig.
410 7A). This result is consistent with the published glycan profile of SARS-CoV-2 spike
411 ECD that most of its glycosylation sites are complex-type or hybrid, except two sites
412 (N234 and N709) which are >80% high-mannose (Fig. 7B).

413

414 Competitive inhibition of FRIL's S protein binding was done with the
415 monosaccharides α -methylmannopyranoside, glucose, galactose and yeast mannan
416 from *Saccharomyces cerevisiae* (Fig. 7C). Results show that as expected, glucose and
417 the α -anomeric configuration of mannose were able to inhibit FRIL binding to S
418 protein, while galactose, which is not a ligand of FRIL, had no such effect. Yeast
419 mannan had only a slight inhibitory effect on FRIL binding, in contrast to single
420 α -anomeric mannose.

421

422 **Discussion**

423 The evolutionary dynamics of sustained influenza virus circulation in a population
424 with pre-existing immunity favors the addition of N-glycans to surface glycoproteins,
425 masking immunogenic epitopes that would otherwise be recognized by the host
426 immune system (Tate et al., 2014). Encountering carbohydrate binding agents that
427 target this “glycan shield” puts the virus in a difficult position, where mutations that
428 delete surface glycans will render the virus more susceptible to antibody recognition,
429 and the addition of glycans increase their vulnerability to lectins. This carbohydrate
430 binding agent concept has been hypothesized as a novel strategy in the treatment of
431 HIV (Balzarini, 2005).

432

433 A panel of 11 influenza viruses showed that FRIL has potent MN effects against
434 group 1, group 2 and influenza B viruses, even strains without heavily N-glycosylated
435 HAs such as WSN (2 sites) and RG32A (3 sites). Only a weak correlation exists
436 between the number of predicted glycans on the virus and its FRIL EC₅₀, indicating
437 that aside from the number of N-glycan sites, the type and position of N-glycans also
438 play a role in FRIL neutralization. The laboratory strain PR8, which does not have any
439 glycosylation on its HA head and has previously been found to be resistant to CVN
440 (O'Keefe et al., 2003), was also resistant to FRIL.

441

442 The discovery that FRIL showed stronger binding to complex type glycans than high
443 mannose was unexpected, as most exogenous lectins that have antiviral properties
444 interact predominantly with high-mannose structures (Mitchell et al., 2017). FRIL has
445 previously been characterized as a mannose/glucose lectin that bound to both α 1-3
446 and α 1-6 linked mannose, but did not precipitate yeast mannans (Mo et al., 1999). Our
447 glycan array results confirm that FRIL binds to single mannose and branched
448 trimannoside as Mo *et al* reported, but also had equal or stronger affinity to various
449 complex type N-glycans, especially those with α 1-3 or α 1-4 fucosylated sub-terminal
450 GlcNAc. It is worth noting that, as Figure 7A, 7C and supplementary Fig S3C
451 suggests, FRIL does not entirely abhor attachment to oligomannose glycans. The
452 binding is just considerably weaker.

453

454 This affinity for complex type glycans may explain why FRIL was able to
455 demonstrate good neutralization against X181 and SARS-CoV-2, but not HIV.
456 Watanabe *et al* have determined that complex and hybrid type glycans comprise 71%
457 of all N-glycosylation on SARS-CoV-2 S protein, with oligomannose and unoccupied
458 taking up the remaining 28% (Watanabe et al., 2020). Our own mass spectrometry
459 results revealed that 62~67% of glycosylation on egg-origin influenza X181 HA were

460 complex type, with 33~38% oligomannose (Tseng et al., 2019), (supplementary Fig
461 S3A). In contrast, HIV-1 JR-FL Env protein N-glycosylation is ~60% oligomannose
462 (Struwe et al., 2018). This could explain why the high mannose binding lectin
463 Griffithsin exhibited a lower EC₅₀ in HIV than coronavirus, while FRIL had the
464 opposite effect. Nevertheless, all three viruses contain a mixture of oligomannose and
465 complex type glycans, so it might be worthwhile to explore the possibility of
466 synergistic combinations of high-mannose lectins with FRIL to cover a broader
467 spectrum of possible oligosaccharides.

468

469 However, this brings up the concern that since complex type N-glycans are commonly
470 expressed on host cell glycoproteins, FRIL given intranasally would bind to host cells,
471 inducing adverse effects. This trepidation can be alleviated by the fact that our *in vivo*
472 challenge experiment at the highest dosage of 2.9 mg/kg/day FRIL was well-tolerated.
473 In contrast, 2 mg/kg/day of CVN treatment was found to be lethal to mice (Smee et al.,
474 2008). Furthermore, previous studies that used an intraperitoneal administration route
475 for FRIL was well-tolerated at dosages as high as 30 mg/kg, and no significant
476 cytotoxicity was observed in A549 and cancer cell lines (Vigneshwaran et al., 2017).

477

478 FRIL's strong binding to antennary Lewis X-carrying N-glycans may offer a possible
479 explanation for previous reports on its ability to preserve hematopoietic or neural
480 progenitor cells in culture (Colucci et al., 1999, Yao et al., 2008). Lewis X, otherwise
481 known as SSEA-1 or CD15, is a known undifferentiation marker found on stem cells.
482 While its active role in embryonic development is still unknown, it has been reported
483 that antennary Lewis X serve as activators of Notch signaling and maintenance of
484 neural stem cell stemness (Yagi et al., 2012). This may explain why Yao *et al* found
485 Notch up-regulated after neuronal progenitor cells were treated with FRIL (Yao et al.,
486 2008).

487

488 A recent report indicates that the molecularly engineered H84T Banlec inhibits
489 influenza virus uncoating at the late endosome/lysosome stage (Covés-Datson et al.,
490 2020). In our current study we observed a similar phenomenon for both the
491 high-mannose binding ConA and the complex type binding FRIL (Fig. 4E,
492 supplementary Fig. S4D), hinting that this might be a common mechanism of
493 anti-influenza action for diverse categories of lectins. However, pre-treatment of cells
494 with FRIL 1 hour before virus infection did not neutralize the virus (Fig. 4B), and the
495 vast majority of FRIL remained extracellular when FRIL was applied to non-infected
496 cells (supplementary Fig S4E), indicating that unlike H84T, FRIL must first bind to
497 the virus particle before being endocytosed. These results, coupled with our finding

498 that FRIL aggregates influenza virions, allows us to put forth a model for FRIL's
499 anti-influenza action (Fig. 5D): FRIL first binds and cross-links virions extracellularly,
500 which results in either large aggregates rapidly cleared by the host immune system, or
501 the FRIL-virus complex is endocytosed into host cells. The FRIL-bound virus is
502 subsequently retained in the late endosome/lysosome and prevented from nuclear
503 entry, until its ultimate degradation 24 hours post-infection. However, there is the
504 possibility that the mechanism for FRIL inhibition of SARS-CoV-2 may be different
505 from influenza virus, given that we did not observe strong N protein signal retained
506 inside cell punctae in FRIL-treated samples, and further investigations will be needed
507 for a more complete mechanistic understanding.

508

509 An issue that remains unresolved in our current study is generating recombinant FRIL.
510 This may or may not cause problems in practical application of this agent, as other
511 antiviral lectins such as H84T Banlec and Q-Griffithsin have used extensive
512 molecular engineering to uncouple mitogenicity (Swanson et al., 2015) or increase
513 oxidation resistance (Corman et al., 2020). We have attempted various approaches
514 including prokaryotic and yeast cells, but so far production of bioactive recombinant
515 FRIL remains elusive. It is possible that FRIL undergoes extensive post-translational
516 processing comparable to the structurally-similar lectin ConA (Chrispeels et al.,
517 1986).

518

519 In conclusion, we found that FRIL is a tetrameric lectin with potent anti-influenza and
520 anti-SARS-CoV-2 activity. It preferentially binds to complex type N-glycans to halt
521 influenza virus entry at the late endosomal stage, and we have demonstrated that FRIL
522 is effective both *in vitro* and *in vivo*. Furthermore, FRIL's neutralizing ability is at
523 least on par with most known antiviral neutralizing monoclonal antibodies. We
524 believe its utility as a preventive or therapeutic agent in influenza and the current
525 COVID-19 pandemic warrants further investigation: for example, to coat it on masks
526 or be included in aerosol mists in a closed space such as an airplane cabin for
527 reducing transmission, or to be used in an inhaler (like Relenza for influenza), which
528 will require vigilant clinical trials to evaluate its safety and efficacy.

529

530 Acknowledgements

531 We thank Sue-Jane Chen and Yung-Chieh Tseng for insightful discussions. We thank
532 Academia Sinica Biological Electron Microscopy Core Facility for EM technical
533 support. The core facility is funded by the Academia Sinica Core Facility and
534 Innovative Instrument Project (AS-CFII-108-119). We thank Academia Sinica
535 Cryo-EM Center (Grant No. AS-CFII-108-110) and Taiwan Protein Project (Grant No.
536 AS-KPQ-109-TPP2). We thank Chien-Hung Chen for glycopeptide liquid
537 chromatography MS/MS analysis, and Tsung-Wei Su for SEC-MALS operation.
538 Funding of this project was provided by Academia Sinica Genomics Research Center
539 Summit Project AS-SUMMIT-109 and Taiwan Ministry of Science and Technology
540 Grant 108-2113-M-001-014 (to C.M.).

541

542 Author Contributions

543 C.M., J.T.J., C.H.W., C.Y.W. and Y.M.L. designed the experiments, C.M. and Y.M.L.
544 wrote the paper, X.C. and Y.M.L. worked on figures and diagrams. J.T.J, S.A.M. and
545 Y.M.L. carried out the initial antiviral screening and animal studies, K.S.L. performed
546 the glycan array, S.A.M. conducted immunofluorescent imaging, J.T.J and Y.M.L. did
547 the MNs and other *in vitro* work, J.M.L. created pseudotyped HIV, T.H.C. performed
548 FRIL EM and 3D reconstruction of FRIL EM images, J.M.L., X.C., Y.M.W. and
549 M.C.H. performed SARS-CoV-2 spike EM and 3D reconstruction of spike EM
550 images.

551

552 Declaration of Interests

553 A patent application has been submitted by Academia Sinica based on the results
554 shown in this study, with C.M., J.T.J. and Y.M.L. as inventors.

555

556 **STAR Methods**557 *Resource availability*

558 Lead contact

559 Further information and requests for resources and reagents should be directed to the
560 Lead Contact, Che Ma (cma@gate.sinica.edu.tw).

561

562 *Materials availability*

563 All unique/stable reagents generated in this study are available from the Lead Contact
564 with a completed Materials Transfer Agreement.

565

566 *Data and code availability*

567 Negative stain EM density of FRIL and cryo-EM map/structure of SARS-CoV-2 spike
568 protein generated during this study have been deposited in the Electron Microscopy
569 Data Bank. Negative stain EM structure of FRIL tetramer (EMD-30380), cryo-EM
570 structure of SARS-CoV-2 spike protein (EMD-30381).

571

572 *Experimental model and subject details*573 *Virus strains*

574 The vaccine strains of A/California/7/2009-like, A/Vietnam/1194/2004-like,
575 A/Victoria/361/2011-like, A/Wisconsin/67/2005-like, A/Shanghai/2/2013-like,
576 B/Brisbane/60/2008-like, B/Florida/04/2006-like, and B/Malaysia/2506/2004-like
577 viruses were obtained from Adimmune Corporation, Taichung, Taiwan. A/WSN/1933,
578 A/New Caledonia/20/1999, and A/Puerto Rico/8/1934 were obtained from National
579 Institute for Biological Standards and Control, Hertfordshire, UK.
580 hCoV-19/Taiwan/NTU04/2020 was obtained from National Taiwan University, Taipei,
581 Taiwan.

582

583 *Plants and cell lines*

584 Madin-Darby canine kidney (CCL-34), A549 (CCL-185) and Vero E6 (CRL-1586)
585 cell lines were obtained from American Type Culture Collection, Manassas, Virginia.
586 The seeds of *Lablab purpureus* were purchased from a market in Hong Kong.

587

588 *Animals*

589 9 day old embryonated chicken eggs were obtained from Animal Health Research
590 Institute, New Taipei City, Taiwan. 8 week old female Balb/c mice were obtained
591 from LASCo, Taipei, Taiwan.

592

593 *Method details*

594 FRIL purification

595 *Lablab purpureus* bean powder was first extracted by PBS, then dialyzed overnight
596 with decreased salt concentration. The sediment was resolubilized in 20 mM
597 phosphate buffer pH 8, and loaded onto an Unosphere Q column (BioRad, Hercules,
598 California). Bound proteins were eluted with a 0~0.5M NaCl gradient, and fractions
599 exhibiting the highest MN titers (peak 2) against RG14 (H5N1) strain were pooled
600 and concentrated. The concentrated sample was then loaded onto a Superdex s200
601 10/300GL size exclusion column (GE, Boston, Massachusetts), and fractions
602 exhibiting the highest MN titers (peak 4) against RG14 were pooled and concentrated.
603 Finally, the 5 bands representing FRIL were separated from 2 nonspecific bands at
604 approximately 30 and 40 kDa by collecting cibaron blue affinity chromatography
605 (Affi-Gel. BioRad) flow-through.

606

607 Microneutralization and plaque reduction assays

608 The 50% infective dose (TCID₅₀) and immunoplaque assay (PFU/ml) of viruses in
609 MDCK or Vero E6 cells were determined beforehand. A protocol for the serological
610 diagnosis of influenza by MN assay was used, with FRIL in place of sera (World
611 Health Organization., 2011). FRIL and viruses were incubated at 37°C for 1 hour in a
612 96 well tissue culture plate, then 1.5x10⁴ cells/well were added to the mixture. The
613 plate was then cultured in serum-free medium for 18~20 hours, then washed and fixed
614 with 50% methanol 50% acetone. Anti-NP (influenza virus) or anti-N (coronavirus)
615 ELISA was then used to determine virus titer. Plates were blocked with 5% skim milk
616 0.5% BSA, and rabbit polyclonal anti-NP or mouse polyclonal anti-N primary
617 antibody and HRP-conjugated secondary antibody were sequentially added.
618 Peroxidase substrate solution (TMB) and 1M H₂SO₄ stop solution were used and the
619 absorbance (OD 450 nm) read by a microplate reader (Victor3. Perkin Elmer,
620 Waltham, Massachusetts).

621 For plaque reduction assay, MDCK or Vero E6 cells were plated onto a 6-well plate at
622 2x10⁵ cells/well overnight for 90% confluence. FRIL and viruses were co-incubated
623 at 37°C for 1 hour, before the mixture is added onto the monolayer for another hour.
624 The virus/FRIL mixture is aspirated, the cells washed with PBS, and a 0.5%
625 low-melting agarose in serum-free media is layered onto the cells. The plates are
626 allowed to solidify at room temperature for 30 minutes, then incubated at 37°C for
627 4~5 days or until cytopathic effects (CPE) are observed. Afterwards, cells are fixed
628 with 7.4% formalin 1% tween 20, and agarose plugs removed. For influenza virus,
629 immunoplaque assay performed with rabbit polyclonal anti-nucleoprotein (NP)
630 primary antibody and HRP-conjugated secondary antibody, and plaques are visualized
631 by incubating with KPL TruBlue peroxidase substrate (Seracare, Milford,

632 Massachusetts) overnight. For coronavirus, the plate was stained with 0.5% crystal
633 violet.

634

635 Production and purification of differentially-glycosylated viruses

636 The method for egg-based production of differentially-glycosylated viruses has been
637 described previously (Tseng et al., 2019). Briefly, 9 day old embryonated chicken
638 eggs were inoculated with A/California/7/2009-like (X181) virus at 10,000-fold
639 dilution of seed stock in allantoic cavity, with or without the presence of 0.2 mg/ml
640 KIF. After 48 hrs incubation (35°C), the allantoic fluid was harvested and
641 concentrated, and half of the KIF-treated virus were subjected to endoglycosidase H
642 (20 µg/ml final concentration) treatment overnight at 4°C. All three treatments (no
643 treatment, KIF, KIF and EndoH) were loaded onto 25x89 centrifugal tubes with a
644 25~55% sucrose gradient, and influenza virus particles purified using sucrose gradient
645 centrifugation (Optima L-90K. Beckman Coulter, Brea, California) at 20000 rpm
646 overnight. Finally, sucrose is removed from the purified viruses through dialysis (10k
647 MWCO Snakeskin tubing. Thermo Fisher Scientific, Waltham, Massachusetts) with
648 PBS.

649

650 Glycan array analysis

651 Glycan array analysis was performed as described previously (Shivatara et al., 2016).
652 Briefly, FRIL was conjugated with Cy3 in a 1:1 ratio, and bioactivity checked with
653 hemagglutination assay. Glycan microarray slides were blocked for 1 hour with
654 blocking buffer (Superblock, Thermo Fisher Scientific) and then washed with PBST
655 (PBS buffer, 0.05% Tween 20). 10 µg/ml conjugated FRIL-Cy3 was added to the
656 array and incubated at room temperature for 1 hour, and washed to remove unbound
657 FRIL. Microarray slides were spun dry prior to scanning with a GenePix 4300A
658 reader (Molecular Devices, San Jose, California) at OD 532 nm and analyzed with
659 GenePix Pro 7.0 software (Molecular Devices).

660

661 FRIL live-virus ELISA and Western Blotting

662 For FRIL ELISA, live sucrose-gradient purified X181 viruses were absorbed onto an
663 empty ELISA plate at 4°C overnight. 10% BSA in PBS was used for blocking, then
664 serially-diluted FRIL was added onto the plate. Polyclonal anti-FRIL primary
665 antibody and HRP-conjugated secondary antibody were sequentially added.

666 Peroxidase substrate solution (TMB) and 1M H₂SO₄ stop solution were used and the
667 absorbance (OD 450 nm) read by a microplate reader (Victor3. Perkin Elmer). All
668 steps up to the addition of stop solution were done in a biosafety cabinet.

669 For Western blotting, purified X181 viruses were loaded onto a 4~15% SDS-PAGE

670 (Bio-Rad) with a non-reducing loading dye, the transferred onto PVDF membrane
671 with semi-dry method (Trans-Blot SD, Bio-Rad). The membrane is blocked with 5%
672 BSA in PBST for 1 hour at room temperature, then 1.2 µg/ml FRIL protein is added.
673 The membrane was then sequentially treated with polyclonal anti-FRIL primary
674 antibody and HRP-conjugated secondary antibody. Finally, Clarity ECL substrate
675 (Bio-Rad) was added for chemiluminescence, and visualized with ImageQuant
676 LAS4000 (GE).

677

678 Intranasal challenge in mice

679 Our mouse challenge experiments were performed by following an intranasal
680 administration method described previously (Sidwell et al., 1998), with some
681 modifications. Briefly, LD₅₀ of the A/California/7/2009-like (X181) virus in BALB/c
682 mice were determined before experiments. Ten 8 week old female Balb/c mice per
683 group were sedated with tiletamine and zolazepam (Zoletil, Virbac, Carros, France)
684 i.p. and given a pre-infection 50 µl intranasal dose of FRIL, at 29 or 2.9 µg/dose.
685 Control group was given PBS. 4 hours after treatment, 5LD₅₀ of X181 virus was given
686 intranasally to all groups. Thereafter, 29 or 2.9 µg/dose of FRIL was given i.n. every
687 12 hours for 8 days, and mice body weight and survival were recorded for 21 days.
688 Intranasal administration of the PBS group was halted after 4 days due to declining
689 condition of mice.

690 All animal experiments were conducted in accordance with the guidelines established
691 by the Institutional Animal Care and Use Committee of Academia Sinica (approval no.
692 18-12-1272), and all procedures were performed by a licensed veterinarian. Animals
693 were humanely sacrificed by CO₂ inhalation at the end of experiment.

694

695 Dynamic light scattering

696 Purified X181 viruses (no treatment, KIF and endo H-treated) were incubated with
697 increasing concentrations of FRIL protein at 37°C for 30 minutes. The mixture was
698 then transferred to a plastic cuvette and measured with Zetasizer Nano-ZS (Malvern
699 Instruments, Malvern, UK).

700

701 SEC-MALS

702 FRIL size exclusion chromatography was performed by running the lectin through a
703 silicon-based BioSEC-3 column (Agilent Technologies, Santa Clara, California), on
704 an Akta FPLC (GE) connected to a three-angle light-scattering detector (mini-DAWN
705 TREOS) and a refractive index detector (Optilab T-rEX, Wyatt Technology, Santa
706 Barbara, California). Data analysis was done with ASTRA.

707

708 Hemagglutination inhibition assay

709 The hemagglutination titer of FRIL was determined beforehand.

710 Methyl- α -D-mannopyranoside, D-galactose, D-glucose and L-arabinose were serially
711 diluted in V-bottom 96-well plates with PBS, 25 μ l/well. 25 μ l of 59 μ g/ml FRIL (4.1
712 HAU) were then added to each well, followed by 50 μ l of 0.5% turkey red blood cells
713 (Jianrong, New Taipei City, Taiwan). After 30 minutes of incubation,
714 hemagglutination inhibition titers were assessed by RBC sedimentation at the bottom
715 of the wells.

716

717 Immunofluorescence microscopy

718 MDCK or Vero E6 cells were seeded onto 35x12mm glass bottom dishes (α plus,
719 Taoyuan City, Taiwan) at 2.75×10^5 cells/ml for 16 hours. Purified X181 or unpurified
720 hCoV-19/Taiwan/NTU04/2020 virus (MOI: 1.2 and 1, respectively) were incubated
721 with 100 μ g/ml (final concentration: 33 μ g/ml) of lectin for 1 hour before the mixture
722 was added to dishes for 1~24 hours of infection. Afterwards, cells were fixed and
723 permeabilized before being immunostained with either rabbit polyclonal anti-NP
724 (1:1000 dilution), mouse polyclonal anti-N (1:1000 dilution), mouse polyclonal anti-S
725 (1:100 dilution), or rabbit polyclonal anti-FRIL (1:10000 dilution) antibody and Alexa
726 Fluor 488-labeled goat anti-rabbit secondary antibody. Counterstaining was
727 performed with DAPI. Samples were analyzed by a Leica TCS SP8X confocal
728 microscope with HC PL APO CS2 63x/1.40 oil immersion lens (Leica AG, Wetzlar,
729 Germany).

730

731 Negative stain electron microscopy

732 For negative stain EM density of the oligomeric FRIL protein, FRIL (18 μ g/mL) was
733 applied for 60 seconds to a carbon-coated 400 mesh copper grid (Electron Microscopy
734 Sciences, Hatfield, Pennsylvania), then negatively stained with 2% uranyl formate for
735 60 seconds. Data was collected under a FEI Tecnai G2 F20 S-TWIN electron
736 microscope (Thermo Fisher Scientific) operating at 120 keV and a magnification of
737 470K that resulted in a pixel size of 2.06 \AA at the specimen plane. Particles selection,
738 2D classification and 3D reconstruction were processed by cisTEM. 67,041 particles
739 were chosen to reconstruct the 3D map using a D2 symmetry. Structural figures were
740 generated by UCSF ChimeraX package.

741 For visualization and counting of virus particle aggregation, sucrose-gradient purified
742 X181 viruses and FRIL were co-incubated at 37°C for 30 minutes. After incubation,
743 samples were diluted with PBS and applied to a carbon-coated 400 mesh copper grid
744 and negatively stained with Nano-W (Nanoprobes, Yaphank, New York). Viruses were
745 observed under transmission electron microscope (JEM-1400. JEOL, Peabody,

746 Massachusetts) operating at 120 kV coupled to a CCD camera (Gatan 895. Gatan,
747 Pleasanton, California). Images were captured by Gatan Digital Micrographic
748 software at the magnifications of 2.6K and 5K. Virus aggregation was quantified by
749 calculating the percentage of virus aggregates captured on 20 images (four corners of
750 5 randomly-chosen intact grids) under 5K magnification.

751

752 Cryo-EM

753 HEK293E (Ebna) and HEK293S cells were used to overexpress the SARS-CoV-2
754 Spike protein (GenBank: YP_009724390.1) ectodomain (14-1209) by transfection
755 with polyethylenimine (PEI) in FreeStyle 293 expression medium (Life technologies)
756 at 37°C with 8% CO₂ for 6 days. The supernatant was harvested and purified using
757 Ni-NTA affinity resin (GE Healthcare) and further purified by size-exclusion
758 chromatography Superose 6 10/300 GL (GE Healthcare) in a buffer containing 20
759 mM Tris pH 8.0 and 100 mM NaCl. 4 µL of fresh purified protein sample (0.48mg/ml)
760 were loaded onto a fresh glow discharged (60 s) holey carbon grid (Quantifoil
761 R1.2/1.3) and plunge freezing with a Vitrobot Mark IV (Thermo Fisher Scientific) at 3
762 second blot time in 4°C and 100% humidity. Automated data collection was
763 performed by the EPU software (Thermo Fisher Scientific) in a Titan Krios G3
764 operating at 300 kV with Gatan BioQuantum energy filter and K2 camera. Total of
765 3,417 micrographs were recorded at magnification of 165,000× (0.82 Å/pixel) with a
766 defocus range between -1.0 µm to -2.5 µm. The total dose rate was approximately 57
767 e-/Å² for 60 frames in a 4.5 s exposure time. Movie alignment, contrast-transfer
768 function (CTF) estimation and particle extraction were carried out using cisTEM
769 (Grant et al., 2018). The particle stacks were transferred to Relion 3.0 (Zivanov et al.,
770 2018) for 2D and 3D classification followed by CTF refinement, 3D auto-refine and
771 post-processing without symmetry. The overall resolution (4.7Å) of cryo-EM map
772 was reported by the gold-standard FSC with 0.143 cut-off. UCSF ChimeraX
773 (Goddard et al., 2018) and Coot (Emsley et al., 2010) were used to fit atomic models
774 (PDB 6VSB) into the final map. The model was manually rebuilt using Coot (Emsley
775 et al., 2010) and subsequently real-space refined by Phenix (Liebschner et al., 2019).
776 N-linked glycans were hand-modeled using Coot Glyco extension based on the
777 published glycan profile (Watanabe et al., 2020). Structure figures were generated
778 using UCSF ChimeraX.

779

780 Trypsin susceptibility assay

781 Trypsin susceptibility assay was performed as described previously (Kadam et al.,
782 2017). Briefly, recombinant A/California/7/2009 HA was diluted to 2 mg/ml in PBS
783 (pH 7.4), and FRIL (FRIL:HA 10:1 or 2:1 molar ratio) or FI6 (2:1 molar ratio) were

784 added and allowed to incubate for 30 minutes at room temperature. A 200 mM sodium
 785 acetate buffer (pH 5) was then added to the mixture to lower the pH down to 5, and
 786 incubated at 37°C for 20 minutes. A 200 mM Tris buffer (pH 8.5) was used to bring
 787 the pH back up to 7. Finally, TPCK-trypsin was added to the mixture at a 1:50 molar
 788 ratio and the mixture incubated at 37°C for 30 minutes before the digestion was
 789 stopped by the addition of SDS-PAGE loading dye (non-reducing), and denatured at
 790 100°C for 10 mins. Samples were run on a 4~15% SDS-PAGE (Bio-Rad) to assess
 791 trypsin susceptibility.

792

793 *Quantification and statistical analysis*

794 All data are presented as mean \pm SEM except Fig 1B and 6B, where only a single
 795 sample was tested against each virus. Absolute EC₅₀ values were calculated with
 796 Prism 8 software. For Fig. 2E significance was determined by log-rank (Mantel-Cox)
 797 test. For Fig. 6E significance vs PBS control was determined by multiple t tests. For
 798 Fig. S3 significance was determined by 2-way ANOVA with Tukey's multiple
 799 comparison. For all data, significance is presented as p<0.05 (*), with p<0.01 (**),
 800 p<0.001 (***) and p<0.0001 (****) indicated by an increasing number of asterisks.
 801 The *n* number of individual experiments are mentioned in figure legends.

802

803 *Key resources table*

REAGENT or RESOURCE	SOURCE	IDENTIFIER
Antibodies		
Rabbit anti-NP polyclonal antibody	This study	N/A
Rabbit anti-FRIL polyclonal antibody	This study	N/A
Mouse anti-SARS-CoV-2 N protein	This study	N/A
Mouse anti-SARS-CoV-2 S protein	This study	N/A
Rabbit anti-LAMP1 polyclonal antibody	abcam	ab24170
Goat anti-Rabbit IgG Alexa Fluor 647	abcam	ab150079
Goat anti-Mouse IgG Alexa Fluor 488	Invitrogen	A32723
Goat anti-Rabbit IgG Alexa Fluor 488	Invitrogen	A32731
Goat anti-Rabbit IgG HRP	Jackson ImmunoResearch	111-035-144
FI6	This study	N/A
Bacterial and Virus Strains		
A/California/7/2009-like	Adimmune	N/A
A/Vietnam/1194/2004-like	Adimmune	N/A
A/Victoria/361/2011-like	Adimmune	N/A

A/Wisconsin/67/2005-like	Adimmune	N/A
A/Shanghai/2/2013-like	Adimmune	N/A
B/Brisbane/60/2008-like	Adimmune	N/A
B/Florida/04/2006-like	Adimmune	N/A
B/Malaysia/2506/2004-like	Adimmune	N/A
A/WSN/1933	NIBSC	N/A
A/New Caledonia/20/1999	NIBSC	N/A
A/Puerto Rico/8/1934	NIBSC	N/A
hCoV-19/Taiwan/NTU04/2020	NTU	N/A
Biological Samples		
<i>Lablab purpureus</i>	Market in Hong Kong	N/A
Chemicals, Peptides, and Recombinant Proteins		
Recombinant A/California/09 (H1N1) hemagglutinin ectodomain	This study	N/A
Recombinant SARS-CoV-2 spike protein ectodomain	This study	N/A
Recombinant endoglycosidase H	This study	N/A
Kifunensine	Sigma-Aldrich	CAS 109944-15-2
DAPI staining solution	abcam	ab228549
Concanavalin A	Sigma-Aldrich	L7647
Mannan from <i>Saccharomyces cerevisiae</i>	Sigma-Aldrich	M7504
Deposited Data		
Negative stain EM structure of FRIL tetramer	This study	EMD-30380
Cryo-EM structure of SARS-CoV-2 spike protein	This study	EMD-30381
Experimental Models: Cell Lines		
Madin-Darby canine kidney	ATCC	CCL-34
A549	ATCC	CCL-185
Vero E6	ATCC	CRL-1586
HEK293T	ATCC	CRL-3216
HEK293S GnTI-	ATCC	CRL-3022
Experimental Models: Organisms/Strains		
Balb/c	LASCo	N/A
Embryonated chicken eggs	AHRI	N/A
Software and Algorithms		

Prism 8.0	Graphpad software	N/A
Image J	NIH	N/A
ChimeraX	UCSF	N/A
cisTEM	Tim Grant, Alexis Rohou, Nikolaus Grigorieff	N/A
Relion	MRC Laboratory, Cambridge, UK	N/A
Coot	Emsley et al.	NA
Phenix	Liebschner et al.	NA
Other		
Turkey red blood cells	Jianrong	N/A

804

805

806 **References and Notes**

- 807 B, S. G., POHLENTZ, G., SCHULTE, M., MORMANN, M. & NADIMPALLI, S. K. 2014.
808 N-glycan analysis of mannose/glucose specific lectin from Dolichos lablab
809 seeds. *Int J Biol Macromol*, 69, 400-7.
- 810 BALZARINI, J. 2005. Targeting the glycans of gp120: a novel approach aimed at the
811 Achilles heel of HIV. *Lancet Infect Dis*, 5, 726-31.
- 812 BALZARINI, J., NEYTS, J., SCHOLS, D., HOSOYA, M., VAN DAMME, E., PEUMANS, W. &
813 DE CLERCQ, E. 1992. The mannose-specific plant lectins from Cymbidium
814 hybrid and Epipactis helleborine and the (N-acetylglucosamine)n-specific
815 plant lectin from Urtica dioica are potent and selective inhibitors of human
816 immunodeficiency virus and cytomegalovirus replication in vitro. *Antiviral Res*,
817 18, 191-207.
- 818 CHRISPEELS, M. J., HARTL, P. M., STURM, A. & FAYE, L. 1986. Characterization of the
819 endoplasmic reticulum-associated precursor of concanavalin A. Partial amino
820 acid sequence and lectin activity. *J Biol Chem*, 261, 10021-4.
- 821 COLUCCI, G., MOORE, J. G., FELDMAN, M. & CHRISPEELS, M. J. 1999. cDNA cloning of
822 FRIL, a lectin from Dolichos lablab, that preserves hematopoietic progenitors
823 in suspension culture. *Proc Natl Acad Sci U S A*, 96, 646-50.
- 824 CORMAN, J. M., HAMORSKY, K. T., SHEPHERD, J. W., HIATT, E., FUQUA, J. L. & PALMER,
825 K. E. 2020. Stability of plasmid and viral banks supporting the cGMP
826 manufacture of Q-Griffithsin from a TMV-based viral vector. *Journal of*
827 *Biotechnology*, 320, 74-76.
- 828 CORTI, D., VOSS, J., GAMBLIN, S. J., CODONI, G., MACAGNO, A., JARROSSAY, D.,
829 VACHIERI, S. G., PINNA, D., MINOLA, A., VANZETTA, F., SILACCI, C.,
830 FERNANDEZ-RODRIGUEZ, B. M., AGATIC, G., BIANCHI, S.,
831 GIACCHETTO-SASSELLI, I., CALDER, L., SALLUSTO, F., COLLINS, P., HAIRE, L. F.,
832 TEMPERTON, N., LANGEDIJK, J. P., SKEHEL, J. J. & LANZAVECCHIA, A. 2011. A
833 neutralizing antibody selected from plasma cells that binds to group 1 and
834 group 2 influenza A hemagglutinins. *Science*, 333, 850-6.
- 835 COVČS-DATSON, E. M., KING, S. R., LEGENDRE, M., GUPTA, A., CHAN, S. M., GITLIN, E.,
836 KULKARNI, V. V., PANTALE *Proceedings of the National Academy of Sciences*,
837 117, 2122-2132.
- 838 GIANCHECCHI, E., TORELLI, A. & MONTOMOLI, E. 2019. The use of cell-mediated
839 immunity for the evaluation of influenza vaccines: an upcoming necessity.
840 *Human Vaccines & Immunotherapeutics*, 15, 1021-1030.
- 841 GORDTS, S. C., RENDERS, M., FERIR, G., HUSKENS, D., VAN DAMME, E. J., PEUMANS,
842 W., BALZARINI, J. & SCHOLS, D. 2015. NICTABA and UDA, two GlcNAc-binding
843 lectins with unique antiviral activity profiles. *J Antimicrob Chemother*, 70,

- 844 1674-85.
- 845 GOWDA, L. R., SAVITHRI, H. S. & RAO, D. R. 1994. The complete primary structure of
846 a unique mannose/glucose-specific lectin from field bean (*Dolichos lab lab*). *J*
847 *Biol Chem*, 269, 18789-93.
- 848 GREIG, A. S. & BOUILLANT, A. M. 1977. Binding effects of concanavalin A on a
849 coronavirus. *Can J Comp Med*, 41, 122-6.
- 850 GURAN, A., TICHA, M., FILKA, K. & KOCOUREK, J. 1983. Isolation and properties of a
851 lectin from the seeds of the Indian bean or lablab (*Dolichos lablab* L.).
852 *Biochem J*, 209, 653-7.
- 853 HAMELRYCK, T. W., MOORE, J. G., CHRISPPEELS, M. J., LORIS, R. & WYNS, L. 2000. The
854 role of weak protein-protein interactions in multivalent lectin-carbohydrate
855 binding: crystal structure of cross-linked FRIL. *J Mol Biol*, 299, 875-83.
- 856 HARTSHORN, K. L., WHITE, M. R., SHEPHERD, V., REID, K., JENSENIUS, J. C. & CROUCH,
857 E. C. 1997. Mechanisms of anti-influenza activity of surfactant proteins A and
858 D: comparison with serum collectins. *American Journal of Physiology-Lung*
859 *Cellular and Molecular Physiology*, 273, L1156-L1166.
- 860 HEO, Y. A. 2018. Baloxavir: First Global Approval. *Drugs*, 78, 693-697.
- 861 HSIEH, L. E., LIN, C. N., SU, B. L., JAN, T. R., CHEN, C. M., WANG, C. H., LIN, D. S., LIN, C.
862 T. & CHUEH, L. L. 2010. Synergistic antiviral effect of *Galanthus nivalis*
863 agglutinin and nelfinavir against feline coronavirus. *Antiviral Res*, 88, 25-30.
- 864 IMAI, M., YAMASHITA, M., SAKAI-TAGAWA, Y., IWATSUKI-HORIMOTO, K., KISO, M.,
865 MURAKAMI, J., YASUHARA, A., TAKADA, K., ITO, M. & NAKAJIMA, N. 2020.
866 Influenza A variants with reduced susceptibility to baloxavir isolated from
867 Japanese patients are fit and transmit through respiratory droplets. *Nature*
868 *microbiology*, 5, 27-33.
- 869 KADAM, R. U., JURASZEK, J., BRANDENBURG, B., BUYCK, C., SCHEPENS, W. B. G.,
870 KESTELEYN, B., STOOPS, B., VREEKEN, R. J., VERMOND, J., GOUTIER, W., TANG,
871 C., VOGELS, R., FRIESEN, R. H. E., GOUDSMIT, J., VAN DONGEN, M. J. P. &
872 WILSON, I. A. 2017. Potent peptidic fusion inhibitors of influenza virus.
873 *Science*, 358, 496-502.
- 874 KEYAERTS, E., VIJGEN, L., PANNECOUQUE, C., VAN DAMME, E., PEUMANS, W.,
875 EGBERINK, H., BALZARINI, J. & VAN RANST, M. 2007. Plant lectins are potent
876 inhibitors of coronaviruses by interfering with two targets in the viral
877 replication cycle. *Antiviral Res*, 75, 179-87.
- 878 KOSZALKA, P., TILMANIS, D. & HURT, A. C. 2017. Influenza antivirals currently in
879 late-phase clinical trial. *Influenza Other Respir Viruses*, 11, 240-246.
- 880 KUMAKI, Y., WANDERSEE, M. K., SMITH, A. J., ZHOU, Y., SIMMONS, G., NELSON, N. M.,
881 BAILEY, K. W., VEST, Z. G., LI, J. K. K., CHAN, P. K.-S., SMEE, D. F. & BARNARD, D.

- 882 L. 2011. Inhibition of severe acute respiratory syndrome coronavirus
883 replication in a lethal SARS-CoV BALB/c mouse model by stinging nettle lectin,
884 *Urtica dioica* agglutinin. *Antiviral Research*, 90, 22-32.
- 885 LOZANO, R., NAGHAVI, M., FOREMAN, K., LIM, S., SHIBUYA, K., ABOYANS, V.,
886 ABRAHAM, J., ADAIR, T., AGGARWAL, R., AHN, S. Y., ALVARADO, M.,
887 ANDERSON, H. R., ANDERSON, L. M., ANDREWS, K. G., ATKINSON, C.,
888 BADDOUR, L. M., BARKER-COLLO, S., BARTELS, D. H., BELL, M. L., BENJAMIN, E.
889 J., BENNETT, D., BHALLA, K., BIKBOV, B., BIN ABDULHAK, A., BIRBECK, G.,
890 BLYTH, F., BOLLIGER, I., BOUFOUS, S., BUCELLO, C., BURCH, M., BURNEY, P.,
891 CARAPETIS, J., CHEN, H., CHOU, D., CHUGH, S. S., COFFENG, L. E., COLAN, S. D.,
892 COLQUHOUN, S., COLSON, K. E., CONDON, J., CONNOR, M. D., COOPER, L. T.,
893 CORRIERE, M., CORTINOVIS, M., DE VACCARO, K. C., COUSER, W., COWIE, B. C.,
894 CRIQUI, M. H., CROSS, M., DABHADKAR, K. C., DAHODWALA, N., DE LEO, D.,
895 DEGENHARDT, L., DELOSSANTOS, A., DENENBERG, J., DES JARLAIS, D. C.,
896 DHARMARATNE, S. D., DORSEY, E. R., DRISCOLL, T., DUBER, H., EBEL, B.,
897 ERWIN, P. J., ESPINDOLA, P., EZZATI, M., FEIGIN, V., FLAXMAN, A. D.,
898 FOROUZANFAR, M. H., FOWKES, F. G., FRANKLIN, R., FRANSEN, M., FREEMAN,
899 M. K., GABRIEL, S. E., GAKIDOU, E., GASPARI, F., GILLUM, R. F.,
900 GONZALEZ-MEDINA, D., HALASA, Y. A., HARING, D., HARRISON, J. E.,
901 HAVMOELLER, R., HAY, R. J., HOEN, B., HOTEZ, P. J., HOY, D., JACOBSEN, K. H.,
902 JAMES, S. L., JASRASARIA, R., JAYARAMAN, S., JOHNS, N., KARTHIKEYAN, G.,
903 KASSEBAUM, N., KEREN, A., KHOO, J. P., KNOWLTON, L. M., KOBUSINGYE, O.,
904 KORANTENG, A., KRISHNAMURTHI, R., LIPNICK, M., LIPSHULTZ, S. E., OHNO, S.
905 L., et al. 2012. Global and regional mortality from 235 causes of death for 20
906 age groups in 1990 and 2010: a systematic analysis for the Global Burden of
907 Disease Study 2010. *Lancet*, 380, 2095-128.
- 908 LUSVARGHI, S., LOHITH, K., MORIN-LEISK, J., GHIRLANDO, R., HINSHAW, J. E. &
909 BEWLEY, C. A. 2016. Binding Site Geometry and Subdomain Valency Control
910 Effects of Neutralizing Lectins on HIV-1 Viral Particles. *ACS Infect Dis*, 2,
911 882-891.
- 912 MAGADAN, J. G., ALTMAN, M. O., INCE, W. L., HICKMAN, H. D., STEVENS, J.,
913 CHEVALIER, A., BAKER, D., WILSON, P. C., AHMED, R., BENNINK, J. R. &
914 YEWDELL, J. W. 2014. Biogenesis of influenza A virus hemagglutinin
915 cross-protective stem epitopes. *PLoS Pathog*, 10, e1004204.
- 916 MATLIN, K. S., REGGIO, H., HELENIUS, A. & SIMONS, K. 1981. Infectious entry
917 pathway of influenza virus in a canine kidney cell line. *The Journal of Cell*
918 *Biology*, 91, 601-613.
- 919 MILLET, J. K., SERON, K., LABITT, R. N., DANNEELS, A., PALMER, K. E., WHITTAKER, G.

- 920 R., DUBUISSON, J. & BELOUZARD, S. 2016. Middle East respiratory syndrome
921 coronavirus infection is inhibited by griffithsin. *Antiviral Res*, 133, 1-8.
- 922 MITCHELL, C. A., RAMESSAR, K. & O'KEEFE, B. R. 2017. Antiviral lectins: Selective
923 inhibitors of viral entry. *Antiviral Res*, 142, 37-54.
- 924 MO, H., MEAH, Y., MOORE, J. G. & GOLDSTEIN, I. J. 1999. Purification and
925 characterization of Dolichos lablab lectin. *Glycobiology*, 9, 173-9.
- 926 O'KEEFE, B. R., GIOMARELLI, B., BARNARD, D. L., SHENOY, S. R., CHAN, P. K.,
927 MCMAHON, J. B., PALMER, K. E., BARNETT, B. W., MEYERHOLZ, D. K.,
928 WOHLFORD-LENANE, C. L. & MCCRAY, P. B., JR. 2010. Broad-spectrum in vitro
929 activity and in vivo efficacy of the antiviral protein griffithsin against emerging
930 viruses of the family Coronaviridae. *J Virol*, 84, 2511-21.
- 931 O'KEEFE, B. R., SMEE, D. F., TURPIN, J. A., SAUCEDO, C. J., GUSTAFSON, K. R., MORI, T.,
932 BLAKESLEE, D., BUCKHEIT, R. & BOYD, M. R. 2003. Potent anti-influenza
933 activity of cyanovirin-N and interactions with viral hemagglutinin. *Antimicrob
934 Agents Chemother*, 47, 2518-25.
- 935 SHIVATARE, S. S., CHANG, S. H., TSAI, T. I., TSENG, S. Y., SHIVATARE, V. S., LIN, Y. S.,
936 CHENG, Y. Y., REN, C. T., LEE, C. C., PAWAR, S., TSAI, C. S., SHIH, H. W., ZENG, Y.
937 F., LIANG, C. H., KWONG, P. D., BURTON, D. R., WU, C. Y. & WONG, C. H. 2016.
938 Modular synthesis of N-glycans and arrays for the hetero-ligand binding
939 analysis of HIV antibodies. *Nat Chem*, 8, 338-46.
- 940 SIDWELL, R. W., HUFFMAN, J. H., BARNARD, D. L., BAILEY, K. W., WONG, M. H.,
941 MORRISON, A., SYNDERGAARD, T. & KIM, C. U. 1998. Inhibition of influenza
942 virus infections in mice by GS4104, an orally effective influenza virus
943 neuraminidase inhibitor. *Antiviral Res*, 37, 107-20.
- 944 SMEE, D. F., BAILEY, K. W., WONG, M. H., O'KEEFE, B. R., GUSTAFSON, K. R., MISHIN, V.
945 P. & GUBAREVA, L. V. 2008. Treatment of influenza A (H1N1) virus infections in
946 mice and ferrets with cyanovirin-N. *Antiviral Res*, 80, 266-71.
- 947 STRUWE, W. B., CHERTOVA, E., ALLEN, J. D., SEABRIGHT, G. E., WATANABE, Y., HARVEY,
948 D. J., MEDINA-RAMIREZ, M., ROSER, J. D., SMITH, R., WESTCOTT, D., KEELE, B.
949 F., BESS, J. W., SANDERS, R. W., LIFSON, J. D., MOORE, J. P. & CRISPIN, M. 2018.
950 Site-Specific Glycosylation of Virion-Derived HIV-1 Env Is Mimicked by a
951 Soluble Trimeric Immunogen. *Cell Reports*, 24, 1958-1966.e5.
- 952 SWANSON, M. D., BOUDREAUX, D. M., SALMON, L., CHUGH, J., WINTER, H. C.,
953 MEAGHER, J. L., ANDRE, S., MURPHY, P. V., OSCARSON, S., ROY, R., KING, S.,
954 KAPLAN, M. H., GOLDSTEIN, I. J., TARBET, E. B., HURST, B. L., SMEE, D. F., DE LA
955 FUENTE, C., HOFFMANN, H. H., XUE, Y., RICE, C. M., SCHOLS, D., GARCIA, J. V.,
956 STUCKEY, J. A., GABIUS, H. J., AL-HASHIMI, H. M. & MARKOVITZ, D. M. 2015.
957 Engineering a therapeutic lectin by uncoupling mitogenicity from antiviral

- 958 activity. *Cell*, 163, 746-58.
- 959 TATE, M. D., JOB, E. R., DENG, Y. M., GUNALAN, V., MAURER-STROH, S. & READING, P.
960 C. 2014. Playing hide and seek: how glycosylation of the influenza virus
961 hemagglutinin can modulate the immune response to infection. *Viruses*, 6,
962 1294-316.
- 963 TSENG, Y. C., WU, C. Y., LIU, M. L., CHEN, T. H., CHIANG, W. L., YU, Y. H., JAN, J. T., LIN,
964 K. I., WONG, C. H. & MA, C. 2019. Egg-based influenza split virus vaccine with
965 monoglycosylation induces cross-strain protection against influenza virus
966 infections. *Proc Natl Acad Sci U S A*.
- 967 VIGNESHWARAN, V., THIRUSANGU, P., VIJAY AVIN, B. R., KRISHNA, V., PRAMOD, S. N.
968 & PRABHAKAR, B. T. 2017. Immunomodulatory glc/man-directed Dolichos
969 lablab lectin (DLL) evokes anti-tumour response in vivo by counteracting
970 angiogenic gene expressions. *Clin Exp Immunol*, 189, 21-35.
- 971 WATANABE, Y., ALLEN, J. D., WRAPP, D., MCLELLAN, J. S. & CRISPIN, M. 2020.
972 Site-specific glycan analysis of the SARS-CoV-2 spike. *Science*, eabb9983.
- 973 WORLD HEALTH ORGANIZATION. 2011. *Manual for the laboratory diagnosis and*
974 *virological surveillance of influenza*, Geneva, World Health Organization.
- 975 WU, C. Y., LIN, C. W., TSAI, T. I., LEE, C. D., CHUANG, H. Y., CHEN, J. B., TSAI, M. H.,
976 CHEN, B. R., LO, P. W., LIU, C. P., SHIVATARE, V. S. & WONG, C. H. 2017.
977 Influenza A surface glycosylation and vaccine design. *Proc Natl Acad Sci U S A*,
978 114, 280-285.
- 979 WU, N. C., YOUNG, A. P., AL-MAWSAWI, L. Q., OLSON, C. A., FENG, J., QI, H., CHEN, S.
980 H., LU, I. H., LIN, C. Y., CHIN, R. G., LUAN, H. H., NGUYEN, N., NELSON, S. F., LI,
981 X., WU, T. T. & SUN, R. 2014. High-throughput profiling of influenza A virus
982 hemagglutinin gene at single-nucleotide resolution. *Sci Rep*, 4, 4942.
- 983 YAGI, H., SAITO, T., YANAGISAWA, M., YU, R. K. & KATO, K. 2012. Lewis X-carrying
984 N-glycans regulate the proliferation of mouse embryonic neural stem cells via
985 the Notch signaling pathway. *J Biol Chem*, 287, 24356-64.
- 986 YANG, J. R., LIN, Y. C., HUANG, Y. P., SU, C. H., LO, J., HO, Y. L., YAO, C. Y., HSU, L. C., WU,
987 H. S. & LIU, M. T. 2011. Reassortment and mutations associated with
988 emergence and spread of oseltamivir-resistant seasonal influenza A/H1N1
989 viruses in 2005-2009. *PLoS One*, 6, e18177.
- 990 YAO, H., XIE, X., LI, Y., WANG, D., HAN, S., SHI, S., NAN, X., BAI, C., WANG, Y. & PEI, X.
991 2008. Legume lectin FRIL preserves neural progenitor cells in suspension
992 culture in vitro. *Clin Dev Immunol*, 2008, 531317.
- 993
- 994

995 **Figures and Tables**

996

997 **Figure 1. The isolation and characterization of FRIL from *Lablab purpureus* extract.** (A) Display of the plant
998 *Lablab purpureus*. (B) Microneutralization of *Lablab purpureus* seed crude aqueous extract against
999 X181 (H1N1), RG14 (H5N1), IVR-165 (H3N2), and RG32A (H7N9) viruses. A single experiment was
1000 performed in this screening. (C) Purified anti-viral reagent exhibits five bands on SDS-PAGE (*left*)
1001 which are confirmed as different truncations of the α - and β -subunits of FRIL by mass spectrometry.
1002 The same sample exhibits only one single band of higher molecular weight on native PAGE (*right*).
1003 Black arrows indicate molecular weights (kD) of the protein ladder for SDS-PAGE, no marker was
1004 used on native PAGE. Data representative of 3 independent experiments. (D) SEC-MALS of purified
1005 FRIL in solution (phosphate buffer) shows a single narrow peak. The MALS trace (black line) indicates
1006 a molecular mass of 112.1 ± 0.8 kDa. Data representative of 2 independent experiments. (E)
1007 Negative-stain EM density of purified FRIL (grey) fitted with its previously solved crystal structure
1008 (PDB code 1qmo) confirms its tetrameric state in solution, with different shades of blue for each
1009 monomer. Representative 2D classes are shown on the right. See also Figure S1A

Figure 2. FRIL exhibits potent broad-spectrum anti-influenza activity *in vitro* and *in vivo*. (A) FRIL plaque reduction assay with H1N1 X181 (A/California/07/2009-like) virus. Data representative of 3 independent experiments performed in triplicate (mean±SEM). See also Figure S2A. (B) FRIL (blue) and bnAb FI6v3 (FI6, orange) MN of (*left*) H1N1 X181 (A/California/07/2009-like), (*middle*) H3N2 IVR-165 (A/Victoria/361/2011-like), and (*right*) an influenza B (B/Brisbane/60/2008-like) vaccine strain. Data representative of 2 independent experiments performed in triplicate (mean±SEM) for each strain. (C) HA phylogenetic tree created with MEGA-X shows microneutralization EC₅₀ values (nM) of FRIL and bnAb FI6v3 (FI6) against 11 representative vaccine and laboratory strains of group 1, group 2 and influenza B viruses. Each block is colored by EC₅₀ values (nM): the darker the color, the higher the neutralizing activity. Data representative of 2 independent experiments performed in triplicate (mean±SEM) for each strain. See also Figure S2B. (D) Treatment schedule of X181 challenge and FRIL administration. 29 or 2.9 µg of FRIL protein was given intranasally to BALB/c mice (*n* = 10) 4 hours before challenge. Influenza virus intranasal challenge was conducted using 5LD₅₀ of X181 virus, and 29 or 2.9 µg of FRIL protein was then given intranasally twice per day for 8 days following challenge. Survival (E) and body weight (F) were tracked for 21 days following influenza virus challenge. Intranasal administration for the PBS group was halted after 4 days due to declining condition of mice. Significance (compared to PBS group) was determined by log-rank (Mantel-Cox) test, *p*<0.0001 (****)

Figure 3. FRIL only binds to and neutralizes influenza viruses with complex type N-glycans. (A) Schematic diagram showing the generation of non-treated (KIF (-) Endo H (-), complex and high mannose type glycans), KIF-treated (KIF (+) Endo H (-), high mannose type glycans only), endo H-treated (KIF (-) Endo H (+), complex and single GlcNAc residues on former high mannose sites) and KIF and endo H-treated (KIF (+) Endo H (+), single GlcNAc residue on all N-glycosylation sites) influenza virus particles. (B) SDS PAGE (*left*) and FRIL immunoblotting (*right*) of non-treated, KIF-treated, and KIF and endo H-treated lysed virus particles. FRIL immunoblotting was done by incubating FRIL with viral proteins transferred onto membrane, followed by detection with anti-FRIL antibodies. Data representative of 3 individual experiments. (C, D and E) Microneutralization assay of non-treated (blue square), endo H-treated (light blue square) KIF-treated (green circle) and KIF and endo H-treated (grey triangle) viruses with FRIL (C), ConA (D), and bnAb FI6v3 (E). Mean \pm SEM of three replicates. (F) (*left*) Glycan array with Cy3-labeled FRIL (blue) and ConA (orange). (*right*) List of the twelve glycans that bound to FRIL with the highest intensity. Symbol Nomenclature for Glycans (SNFG) is used to represent oligosaccharides on graph (blue square for GlcNAc, green circle for mannose, yellow circle for galactose, red triangle for fucose and purple diamond for NeuAc). Data representative of 2 independent experiments performed in triplicate (mean \pm SEM).

Figure 4. FRIL halts influenza virus entry in the late endosome. (A) (*upper*) Hemagglutination inhibition of 59 $\mu\text{g/ml}$ FRIL (4 HAU) by the monosaccharides α -methylmannopyranoside (green circle), D-galactose (grey circle), D-glucose (blue circle) and L-arabinose (green star). Panel representative of three replicates. (*lower*) Competitive FRIL microneutralization inhibition with the same monosaccharides as the upper panel. Mean \pm SEM of three replicates. (B) FRIL microneutralization where FRIL and virus were added, either together (circle) or sequentially (square), in a 1 hour pre-treatment step after which they are removed or an ensuing 18 hour incubation step. Mean \pm SEM of three replicates. (C) FRIL microneutralization with a 1 hour low-temperature arrest of viral endocytosis, separating viral entry steps into attachment (black circle), internalization (blue square), and infection (grey triangle), with FRIL added during the different steps. Data representative of 3 independent experiments performed in triplicate (mean \pm SEM). (D) Progression of influenza RNP after virion endocytosis with or without FRIL inhibition, visualized by immunofluorescence tracking of viral NP protein (anti-NP, green) and nuclei (DAPI, blue). Quantification of upper panel plus two others for the percentage of FRIL-treated (blue) and PBS-treated (grey) cells with nuclear NP signal is shown in the bottom panel. Error bars represent SEM. Data representative of 3 independent experiments. (E) (*top panel*) higher magnification showing NP signal (anti-NP, green) clustered in the perinuclear region at 4 hpi for FRIL, as opposed to (*middle panel*) RNP entry into cell nucleus (DAPI, blue) for PBS control. (F) Co-localization (yellow) of influenza NP signal (green) with the late endosomal marker LAMP-1 (red) is observed in FRIL-treated cells at 4 hpi (upper panel) but not in PBS control (lower panel). Data representative of 2 independent experiments.

Figure 5. FRIL aggregates influenza virus particles. (A) Dynamic light scattering (DLS) analysis of virus particle aggregation under increasing concentrations of FRIL (from 1.5 $\mu\text{g/ml}$ in purple line to 490 $\mu\text{g/ml}$ in dark red line) (B) Negative stain EM images of purified X181 virions alone (*upper panels*) and aggregated X181 virus particles after mixing with 150 $\mu\text{g/ml}$ FRIL (*lower panels*). Data representative of 3 independent experiments. (C) Quantitation of aggregated virions calculated from 20 images for each FRIL concentration. Virions that directly contact each other are considered aggregated. Concentrations above 32 $\mu\text{g/ml}$ proved difficult to ascertain due to formation of large overlapping aggregates. (D) A proposed model for FRIL's anti-influenza mechanism: large FRIL/virus aggregations may occur outside the cell to prevent virus entry, while FRIL endocytosed together with the virus may trap the virus in the late endosome and prevent its nuclear import.

Figure 6. FRIL exhibits potent neutralization of SARS-CoV-2. (A) FRIL inhibition of Vero E6 CPE under 100 TCID₅₀ of SARS-CoV-2 (hCoV-19/Taiwan/NTU04/2020). Black triangles represent areas of focal CPE, while FRIL concentrations below 0.78 µg/ml (6.96 nM) were unable to prevent diffuse and widespread CPE. Data representative of 2 experiments. (B) FRIL plaque reduction neutralization assay with hCoV-19/Taiwan/NTU04/2020 virus. A single experiment was performed. See also Figure S6B. (C) FRIL MN of hCoV-19/Taiwan/NTU04/2020. Data representative of 2 experiments performed in quadruplicate (mean±SEM). (D) Immunofluorescence tracking of SARS-CoV-2 (hCoV-19/Taiwan/NTU04/2020) N (green) and S protein (cyan) production 4 to 24 hpi, with or without 33 µg/ml (0.29 µM) FRIL inhibition. Nuclei are counterstained with DAPI (blue). Data representative of 2 experiments. (E) N protein positive cells at different time points after infection, with (blue bars) or without (grey bars) 33 µg/ml (0.29 µM) of FRIL. Three images with 519~1279 cells per image were quantified using ImageJ software. Significance vs PBS control was determined by multiple t tests with Prism 8 software (** p<0.01, *** p<0.001). See also Figure S6C.

Figure 7. FRIL binds to spike protein via complex-type glycans. (A) ELISA of FRIL binding to SARS-CoV-2 S protein, with either native N-glycosylation (containing complex type, hybrid and high mannose glycans, blue square) or high mannose only (green circle). The unglycosylated bovine serum albumin (BSA, grey triangle) was used as control. Mean \pm SEM of three replicates. **(B)** Cryo-EM structure of SARS-CoV-2 Spike protein modeled with glycans according to either the published glycan profile (left, native) or the high-mannose (Man5) type produced by HEK293S cell line (right). Glycans were colored by blue (>50% complex or hybrid) or green (>50% oligomannose). See also Figure S7. **(C)** ELISA values of 10 μ g/ml FRIL under competitive inhibition from the monosaccharides α -methylmannopyranoside (green), D-glucose (blue) and D-galactose (grey), and yeast mannan from *Saccharomyces cerevisiae* (orange). Mean \pm SEM of three replicates.

Highlights

- FRIL is a plant lectin with potent anti-influenza and anti-SARS-CoV-2 activity.
- FRIL preferentially binds to complex type N-glycans on viral glycoproteins.
- FRIL inhibits influenza virus entry by sequestering virions in late endosomes.
- Intranasal administration of FRIL protects against lethal H1N1 challenge in mice.

eTOC blurb

Liu *et al.* demonstrate that FRIL, a plant lectin isolated from the hyacinth bean, has potent antiviral activity against SARS-CoV2 and diverse influenza virus strains. FRIL is effective *in vivo* against H1N1. FRIL's antiviral activity is mediated by binding to complex type N-glycans on viral glycoproteins, interfering with viral entry.

